Ab Initio Study on One-Way Photoisomerization of the Maleic Acid and Fumaric Acid Anion Radical System as a Model System of Their Esters

Masato Sumita and Kazuya Saito*

Department of Chemistry, Graduate School of Pure and Applied Sciences, University of Tsukuba, Tsukuba 305-8571, Japan

Received: July 11, 2006; In Final Form: September 7, 2006

Potential energy surfaces (PESs) of the maleic acid anion radical ($MA^{-\bullet}$: cis isomer)/fumaric acid anion radical ($FA^{-\bullet}$: trans isomer) system as a model system of their esters have been studied in detail using CASSCF method. The results suggest the following: The photoisomerization is initiated with the H−C−C−H dihedral angle distortion [hydrogen out of plain (HOOP) motion] on the D_1 PES. The C−C−C−C dihedral angle distortion occurs on the D_0 PES after the deactivation from D_1 to D_0. A large fraction of the net motion along the isomerization coordinate occurs on the D_0 PES. The D_0 state is responsible for the one-way nature of the photoisomerization.

1. Introduction

In recent years, theoretical chemistry has shown the ubiquitous existence of conical intersections (real crossings between the same spin multiplicity states) where the radiationless decay of electronically excited state occurs.[1] The conical intersection (CI) provides an efficient decay from the excited state to the ground state in a barrierless, ultrafast manner. Many ultrafast photochemical and photophysical phenomena have been understood by considering the existence of CIs. However, the role of CI is not limited to these ultrafast processes. The decay via CI produces vibrationally hot molecules in the ground state.[1,2] In other words, CI plays a role to transform photoenergy to vibrational energy. This vibrational energy can contribute to "thermal" reaction in ground states. The reachable CI that is close to the Franck−Condon (FC) energy may consequently enhance the "thermal" reaction.

A degeneracy point (DP), which is an apex of CI, is not an isolated point on the *n*-dimensional potential energy surface (*n* is the number of vibrational degrees of freedom of the molecule). DPs make a $(n - 2)$-dimensional space called a conical intersection hyperline or seam.[3,4] Methods have been developed to compute structures of the lowest energy DP (LEDP) in the conical intersection hyperline.[5−7] The LEDP on the hyperline has often been interpreted as a photochemical funnel. However, recent calculations demonstrate that excited molecules can reach a hyperline before reaching a LEDP.[8] Furthermore, available product via excited state depends on where the excited molecules transit to the ground state in the conical intersection hyperline.[9] This suggests the importance of exploring the hyperline, which has the possibility to expand the variety of photochemistry and its processes. We have already succeeded in exploring one-dimensional section of the hyperline in some systems that lies at lower energy than the FC one and may be involved in photochemistry.[10,11]

Involvement of CI in cis ↔ trans photoisomerization of some molecules has been pointed out.[12] The influence of the hyperline for this type of photochemistry has, however, not been fully clarified yet. Torikai et al.[13] detected the cis ↔ trans photoisomerization for dimethyl maleate (DMM) and dimethyl fumarate (DMF), and their anion radicals. The photoisomerization process of such neutral species is believed to involve a CI similar to that in ethylene.[12a] The CI in ethylene is very complicated because decoupling of only two electrons causes an avoided crossing between the ground state (S_0) and first excited state (S_1). To reach a S_1/S_0 CI, two more electrons must be decoupled.[12b]

Although cis ↔ trans photoisomerization in radical species is understood more easily than neutral species from a theoretical viewpoint, experimental results on radical species are rare. The photochemistry of maleate anion radicals and fumarate anion radicals and their ester systems is such a rare example. It has been studied in 2-methyltetrahydrofuran (MTHF)[13] and in aqueous solutions.[14] The experiment in MTHF was mainly reported on dimethyl maleate anion radical ($DMM^{-\bullet}$). When $DMM^{-\bullet}$, which is produced by γ-lay irradiation absorption in MTHF at 77 K, is illuminated with UV light, the isomerization occurs. Namely, after excitation of $DMM^{-\bullet}$ with 345 nm lights, the absorption band shifts to 335 nm. This new absorption indicates the formation of the dimethyl fumarate anion radical ($DMF^{-\bullet}$). On the other hand, the absorption band of $DMF^{-\bullet}$ does not change before and after illumination. These observations show that the isomerization occurs only in the direction of the cis → trans. The same (cis → trans) selectivity was also observed in the isomerization reaction of other radical anions such as stilben anion radical.[15] It is noteworthy that a similar cis → trans one-way isomerization was reported for the $DMM^{-\bullet}$/$DMF^{-\bullet}$ system even without UV light illumination at room temperature.[16,17]

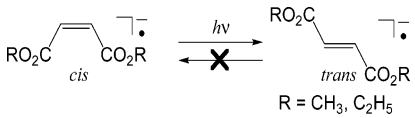

In this work, we have studied the reaction, $MA^{-\bullet} \rightarrow FA^{-\bullet}$ (cis → trans), as a model system of the one-way photoisomerization $DMM^{-\bullet} \rightarrow DMF^{-\bullet}$ by the complete active space self-consisted field (CASSCF) method to elucidate the mechanism of the photoisomerizations.

* Corresponding author. E-mail: kazuya@chem.tsukuba.ac.jp.

10.1021/jp064377o CCC: $33.50
Published on Web 10/17/2006

A few comments are now in order on the potential energy surfaces of the $MA^{-\bullet}/FA^{-\bullet}$ system. The potential energy surfaces of ethylene anion and cation radicals[18] have a symmetry-required conical intersection[3,19] (Jahn−Teller effect) between the ground doublet state (D_0) and the lowest excited state (D_1) at D_{2d} symmetry (90° twist) because both the D_1 and D_0 states belong to degenerate representation (^2E). Because symmetry-required conical intersections simply change into symmetry-allowed conical intersections[3,19] along appropriate geometrical distortion or substitution, it is naturally expected that olefin ion radicals undergo photochemical double-bond rotation through the corresponding conical intersection near 90° twist. Indeed, as described in this paper, for the case of the model $MA^{-\bullet}/FA^{-\bullet}$ system, the lowest point on the D_1 surface coincides with the D_1/D_0 LEDP at approximately 90° twist. However, this does not explain the one-way character of the $MA^{-\bullet} \rightarrow FA^{-\bullet}$ photoisomerization. The purpose of this work is to elucidate the factor that brings one-way photoisomerization and the influence of the hyperline. In our previous work, we investigated the D_1/D_0 hyperline along the central C−C bond twisting for this system.[10] It had been suggested that the difference in steepness of the D_1/D_0 hyperline between the cis and trans sides could be responsible for the one-way isomerization. However, exploring the D_1 and D_0 potential energy surfaces (PESs) in detail, we have arrived at a new conclusion. Upon the cis ↔ trans isomerization, two dihedral angles (i.e., C−C−C−C and H−C−C−H) have to change. Although the simultaneous changes of the two dihedral angles are intuitively plausible, separate changes in C−C−C−C and H−C−C−H are also possible. As shown in this paper, we have concluded that large geometrical change on the D_1 potential energy surface is the H−C−C−H dihedral angle distortion whereas the D_0 potential energy surface is responsible for the C−C−C−C dihedral angle rotation. This mechanism is similar to a conclusion in a recent femtosecond-stimulated Raman spectroscopic study of the light-induced 11-cis and all-trans isomerization of retinal in the visual pigment rhodopsin.[20] This report concluded that the decay from the excited state through a conical intersection is largely mediated by fast hydrogen-out-of-plane (HOOP) motion.

2. Computational Detail

On the neutral species, DMM/DMF and MA/FA, there are some researches about equilibrium structure in ground state through infrared and Raman spectroscopy and theoretical calculation.[21] On anion radical species, however, experimental results are rare. Only a limited method of experiments provides us the information about their equilibrium conformations. The electron spin resonance on $DMM^{-\bullet}$ and $DMF^{-\bullet}$ ruled out the asymmetric conformation with respect to original double bonds.[22] No theoretical studies have been reported concerning the stable conformation of $DMM^{-\bullet}$ and $DMF^{-\bullet}$ in the doublet ground (D_0) state.

First of all, to see the most stable structure of $DMM^{-\bullet}$ and $DMF^{-\bullet}$ in the D_0 state, we carried out the geometry optimization by UB3LYP with the 6-31G* basis set for as many conformations as we can imagine. All calculations in this paper were performed using GAUSSIAN98.[23] Details of resultant equilibrium geometries are given in the Supporting Information. On the basis of these results, the conformations of $MA^{-\bullet}/FA^{-\bullet}$ shown in Figure 1 are adopted as a model system of $DMM^{-\bullet}/DMF^{-\bullet}$.

The D_0 state and first excited doublet state (D_1; $^1(\pi,\pi^*)$) potential energy surfaces were computed with the CASSCF method with the cc-pVDZ basis set. To compare energies of stationary points and DPs where the two-root state-averaged orbital is needed (0.5 weights), the energy of the stationary points on the D_1 surface or D_0 surface that were located with the single-state CASSCF were recalculated using the state-averaged orbital. An intuitive choice of active space for describing the D_1 and D_0 states of the investigated system would be eleven electrons in eight π molecular orbitals, which we refer to as CAS(11,8). However, we found that, for the planar D_0 and D_1 states of $MA^{-\bullet}$ and $FA^{-\bullet}$, CAS(11,8) can be truncated to CAS(7,6) because two of the eight π molecular orbitals are almost doubly occupied (>1.99), corresponding to the OH oxygen lone pairs. Thus, seven electrons in six π molecular orbitals [CAS(7,6)], which corresponds to the π system of the O=C−C=C−C=O moiety, were used as the active space throughout this paper. This active space reduction did not affect to describe the detail of the D_1 and D_0 PESs.

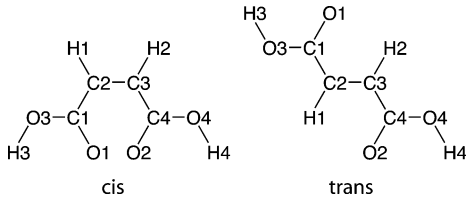

Figure 1. Conformation of $MA^{-\bullet}/FA^{-\bullet}$ (with atomic numbering) as a model system of $DMM^{-\bullet}/DMF^{-\bullet}$

TABLE 1: CASSCF/cc-pVDZ Energies for the D_0 and D_1 Stationary Points and LEDP

species	symmetry	state	E^a	$E_0{}^b$	$E_1{}^c$	$E_{rel}{}^d$
$MA^{-\bullet}$	C_{2v}	D_0 ($^2A_2$)	−453.34113	−453.33869	−453.18538	0
$FA^{-\bullet}$	C_{2h}	D_0 (^2B_g)	−453.35691	−453.35450	−453.20262	−9.9
$MA^{-\bullet}$	C_{2v}	D_1 ($^2B_1$)	−453.20480	−453.32230	−453.20282	85.2
$FA^{-\bullet}$	C_{2h}	D_1 (^2A_u)	−453.22292	−453.33702	−453.22087	73.9
LEDP	C_2	D_1/D_0 ($^2A/^2B$)		−453.28991	−453.28991	30.5
TS	C_1	D_0 (^2A)	−453.3116	−453.2938	−453.2773	28.2

[a] Single-state energy in au. [b] State-averaged energy (au) of the D_0 state. [c] State-averaged energy (au) of the D_1 state. [d] Relative energy with respect to $MA^{-\bullet}$.

3. Results and Discussion

The energies of the D_0 and D_1 ($^1(\pi,\pi^*)$) stationary points and the D_1/D_0 LEDP are listed in Table 1, and their geometrical parameters, in Table 2. The atomic numbering scheme is shown in Figure 1. The C1−C2−C3−C4 and H1−C2−C3−H2 dihedral angles are denoted by θ_1 and θ_2, respectively. Figure 2 shows a schematic representation of the D_0 and D_1 PESs revealed by the present calculations.

3.1. D_0 and D_1 Stationary Points and LEDP. We optimized the D_0 geometries of $MA^{-\bullet}$ and $FA^{-\bullet}$ within C_{2v} and C_{2h} symmetries, respectively. Their stability was confirmed by vibrational analysis. The D_0 states of these geometries are dominated by a single configuration, which is $(3b_1)^2(3a_2)^1$ for $MA^{-\bullet}$ (94.8%) and $(3a_u)^2(3b_g)^1$ for $FA^{-\bullet}$ (95.3%). The central C−C bond (C2−C3) is slightly longer in $MA^{-\bullet}$ (1.410 Å) than in $FA^{-\bullet}$ (1.403 Å). The very large C1−C2−C3 and C2−C3−C4 bond angles of $MA^{-\bullet}$ (131.6°) are ascribed to the repulsion between carbonyl oxygen lone pairs.

Before seeing the excited state of $MA^{-\bullet}$ and $FA^{-\bullet}$ through CAS(7,6), we have checked the relative ordering of states by single-point time-dependent DFT (TDDFT) using B3LYP on the optimized CAS(7,6)/cc-pVDZ D_0 minimum structure of $MA^{-\bullet}$ and $FA^{-\bullet}$.

From the TDDFT/cc-pVDZ result in $MA^{-\bullet}$, the first valence excited state of $MA^{-\bullet}$ is not the $^1(\pi,\pi^*)$ (corresponding to

$3b_1 \rightarrow 3a_2$) but $^1(n,\pi^*)$ ($12b_2 \rightarrow 3a_2$). These energies of $^1(n,\pi^*)$ and $^1(\pi,\pi^*)$ from the D_0 state were computed to be 361 and 339 nm, in terms of wavelength, respectively (energy difference between them is only 3.4 kcal mol^{-1}). By slight distortion of θ_1 or θ_2, the state corresponding to $^1(\pi,\pi^*)$ excitation becomes the first excited state (D_1). The intersection between $^1(\pi,\pi^*)$ and $^1(n,\pi^*)$ is thus expected at small values of θ_1 and θ_2, though it was not located in this work. On the other hand, the first valence excited state of $FA^{-\bullet}$ is $^1(\pi,\pi^*)$ (corresponding to $3a_u \rightarrow 3b_g$) whose transition energy is computed to be 341 nm from the D_0 state. On the other hand, according to the result of TDDFT/aug-cc-pVDZ, the first valence excited state became $^1(\pi,\pi^*)$ in both $MA^{-\bullet}$ and $FA^{-\bullet}$. These suggest that the $^1(\pi,\pi^*)$ is relevant to the photochemistry of this system.

Four low-lying Rydberg states were also exhibited between D_0 state and the first valence excited state in TDDFT/aug-cc-pVDZ. The energies of transition to the four low-lying Rydberg states are computed to be in the region 772−489 nm for both $MA^{-\bullet}$ and $FA^{-\bullet}$. The UV spectrum in MTHF and aqueous solution[13,14] does not exhibit distinct peaks or shoulders in the region 500−300 nm except for 400 (shoulder) nm, 350 nm (peak), and 335 nm (peak), which would be ascribed to $^1(n,\pi^*)$, $^1(\pi,\pi^*)$ of $MA^{-\bullet}$, and $^1(\pi,\pi^*)$ of $FA^{-\bullet}$, respectively. In this paper, therefore, we ignored the effect by these Rydberg states and considered valence excited-state only.

Going back to the result of CAS(7,6), the vertical (Franck−Condon; FC) D_1 states are also dominated by a single configuration, which is $(3b_1)^1(3a_2)^2$ (89.4%) for $MA^{-\bullet}$ and $(3a_u)^1(3b_g)^2$ for $FA^{-\bullet}$ (90.9%), corresponding to the single excitation from the highest doubly occupied molecular orbital to the singly occupied molecular orbital (SOMO). The vertical excitation energies of $MA^{-\bullet}$ and $FA^{-\bullet}$ were calculated to be 96.2 and 95.3 kcal mol^{-1}, respectively (state-averaged calculation). These are overestimated compared to the experimental values in aqueous solution (82.2 and 86.6 kcal mol^{-1}, respectively[14]). This is anticipated because the CASSCF method is known to emphasize the character of the originally unoccupied orbitals.[24] The lack of dynamic electron correlation (especially $\sigma-\pi$ correlation in the present case) in the CASSCF calculation can also be responsible for this discrepancy. The blue shift on going from $MA^{-\bullet}$ to $FA^{-\bullet}$ was not reproduced by the present calculation, too. However, these discrepancies do not alter our conclusion on the cause of the $MA^{-\bullet} \rightarrow FA^{-\bullet}$ one-way isomerization.

The antibonding orbital between the two central carbons, C2 and C3, is doubly occupied and is the main configuration in the D_1 FC state. This means the effect of the antibonding character is strong on the D_1 PES. Indeed, the D_1 PES already has a negative curvature at the FC geometries in the direction of the rotation around the C2−C3 bond. This is in contrast to the case of the lowest excited singlet (S_1) state of retinal protonated Schiff base (RPSB) models,[25] where the negative curvature for double-bond rotation is encountered only after bond-length relaxation. In the case of $MA^{-\bullet}$ and $FA^{-\bullet}$, if there is no constraint, the rotation around the C2−C3 bond would start just after the excitation to the D_1 state.

The D_1 geometry optimizations in C_{2v} and C_{2h} symmetries resulted in elongation of the C2−C3 bond (Table 2). The optimized D_1 geometries of $MA^{-\bullet}$ and $FA^{-\bullet}$ are lower in energy than the corresponding FC geometries by 10.9 and 11.5 kcal mol^{-1}, respectively. Although free molecules does not pass these optimized D_1 geometries, the property of these optimized D_1 geometries will be reflected in the dynamics of excited molecules in the limited space as in MTHF glass.

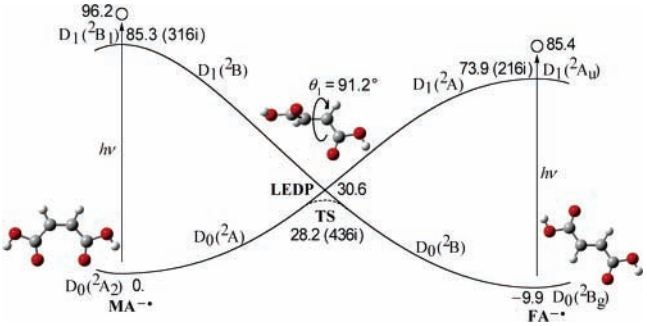

Figure 2. Schematic representation of the D_0 and D_1 potential energy surfaces for the $MA^{-\bullet}/FA^{-\bullet}$ system with energies in kcal mol^{-1}. Open circles indicate Franck−Condon points. The imaginary frequencies are given in parentheses (in cm^{-1}).

TABLE 2: Geometrical Parameters of the Optimized Structures

	$MA^{-\bullet}$ (D_0)	$FA^{-\bullet}$ (D_0)	$MA^{-\bullet}$ (D_1)	$FA^{-\bullet}$ (D_1)	LEDP	TS
Bond Lengths (Å)						
C2−C3	1.410	1.403	1.544	1.536	1.449	1.466
C1−C2	1.425	1.419	1.386	1.380	1.422	1.385
C3−C4	1.425	1.419	1.386	1.380	1.422	1.462
C1−O1	1.212	1.219	1.240	1.248	1.216	1.232
C4−O2	1.212	1.219	1.240	1.248	1.216	1.202
C1−O3	1.386	1.376	1.397	1.385	1.378	1.389
C4−O4	1.386	1.376	1.397	1.385	1.378	1.365
C2−H1	1.083	1.080	1.082	1.077	1.087	1.083
C3−H2	1.083	1.080	1.082	1.077	1.087	1.091
O3−H3	0.946	0.947	0.946	0.946	0.947	0.946
O4−H4	0.946	0.947	0.946	0.946	0.947	0.947
Bond Angles (deg)						
C3−C2−C1	131.6	122.8	131.6	120.8	123.5	120.8
C2−C3−C4	131.6	122.8	131.6	120.8	123.5	124.8
C2−C1−O1	131.9	129.1	130.8	126.6	129.5	130.1
C3−C4−O2	131.9	129.1	130.8	126.6	129.5	128.3
C2−C1−O3	111.4	113.6	113.2	116.5	113.3	114.2
C3−C4−O4	111.4	113.6	113.2	116.5	113.3	112.8
O1−C1−O3	116.8	117.3	116.0	116.9	117.2	115.7
O2−C4−O4	116.8	117.3	116.0	116.9	117.2	118.9
C3−C2−H1	115.4	119.9	113.4	118.6	121.6	119.6
C2−C3−H2	115.4	119.9	113.4	118.6	121.6	123.1
C1−C2−H1	113.0	117.3	115.0	120.6	114.9	119.6
C4−C3−H2	113.0	117.3	115.0	120.6	114.9	112.1
C1−O3−H3	104.1	104.5	103.8	104.3	104.5	103.0
C4−O4−H4	104.1	104.5	103.8	104.3	104.5	105.8
Dihedral Angles (deg)						
C1−C2−C3−C4	0.0	180.0	0.0	180.0	91.23	88.274
H1−C2−C3−H2	0.0	180.0	0.0	180.0	89.27	88.64
C3−C2−C1−O1	0.0	0.0	0.0	0.0	0.448	0.775
C2−C3−C4−O2	0.0	0.0	0.0	0.0	0.448	3.941
C3−C2−C1−O3	180.0	180.0	180.0	180.0	179.7	179.4
C2−C3−C4−O4	180.0	180.0	180.0	180.0	179.7	−177.2
C1−C2−C3−H2	180.0	0.0	180.0	0.0	−89.75	−91.18
H1−C2−C3−C4	180.0	0.0	180.0	0.0	−89.75	−91.91
H1−C2−C1−O1	180.0	180.0	180.0	180.0	−178.6	−179.1
H2−C3−C4−O2	180.0	−180.0	180.0	−180.0	−178.6	−176.5
H1−C2−C1−O3	0.0	0.0	0.0	0.0	0.706	−0.448
H2−C3−C4−O4	0.0	0.0	0.0	0.0	0.706	2.305
C2−C1−O3−H3	180.0	180.0	180.0	180.0	179.5	180.0
C3−C4−O4−H4	180.0	−180.0	180.0	−180.0	179.5	179.4
O1−C1−O3−H3	0.0	0.0	0.0	0.0	−1.184	−1.450
O2−C4−O4−H4	0.0	0.0	0.0	0.0	−1.184	−1.705

Vibrational analyses showed that both the optimized planar D_1 geometries also have an imaginary frequency (316i cm^{-1} for $MA^{-\bullet}$ and 216i cm^{-1} for $FA^{-\bullet}$) corresponding to the C2−C3 rotation. The eigenvector of these imaginary vibrational frequencies are shown in Figure 3. Both the D_1 states of $MA^{-\bullet}$ ($^2B_1$ in C_{2v}) and $FA^{-\bullet}$ (^2A_u in C_{2h}) are then stabilized by rotation around the C2−C3 bond. This lowers the molecular symmetry to C_2, in which the D_1 states of $MA^{-\bullet}$ and $FA^{-\bullet}$ become ^2B and ^2A, respectively. As shown in Figure 3, H1−C2−C3−H2

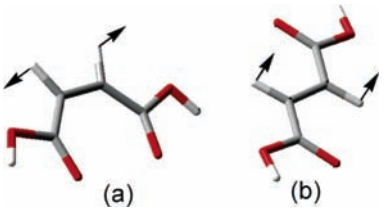

Figure 3. Three-dimensional description of vibration modes having imaginary frequencies [(a) 316i cm^{-1} and (b) 216i cm^{-1}] of the planar optimized structures on the D_1 PES.

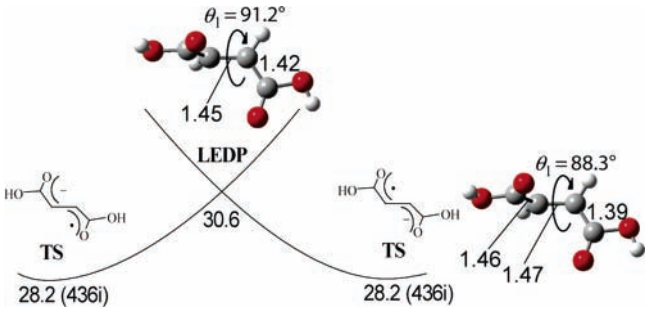

Figure 4. Transition states (TSs) of the cis ↔ trans isomerization are symmetrically located near the LEDP with different charge-spin separation (i.e., "minus-dot" and "dot-minus"). Relative energies are given in kcal mol^{-1}. The imaginary frequencies (cm^{-1}) are shown in parentheses.

dihedral angle distortion is the most dominant component in the imaginary modes. Namely, the rotation around the C2−C3 bond while H1−C2−C1−C3 (H2−C3−C4−C1) plane is maintained does not occur. Therefore, it is necessary to explore the D_1 PES along not only the C1−C2−C3−C4 dihedral angle (θ_1) but also the H1−C2−C3−H2 dihedral angle (θ_2) under C_2 symmetry. We show the D_1 and D_0 PESs along θ_2 later.

Geometry optimizations in C_2 symmetry (switching to optimization using state-averaged orbitals and then to DP optimization was necessary) ultimately led to a DP between the D_1 and D_0 (^2B and ^2A) states in which the C2−C3 bond is twisted by ca. 91.2° (Table 2 and Figure 2). An optimization in C_1 symmetry resulted in the same DP, which confirms that the DP of C_2 symmetry near the 90° twist is indeed the LEDP (i.e., a "true minimum" on the D_1/D_0 hyperline). This perpendicular DP simply originates from the fact that, in C_2 symmetry, the $3b_1$ (bonding) and $3a_2$ (antibonding) orbitals of $MA^{-\bullet}$ exchange with the $3b_g$ (antibonding) and $3a_u$ (bonding) orbitals of $FA^{-\bullet}$, respectively (see ref 26 for similar situations in olefin cation radicals). The LEDP is to be the lowest point on the D_1 surface. A similar perpendicular LEDP has been located for penta-2,4-dieniminium (PDI), which is the model molecule of RPSB.[25]

The gradient difference (GD) vector of the present LEDP, which must be totally symmetric, corresponds to the C2−C3 rotation whereas the derivative coupling (DC) vector, which is symmetry-lowering, has an effect of separating the negative charge and the unpaired spins into the two molecular halves. In the direction of the DC vector, we have located the D_0 transition state (TS) of cis−trans adiabatic isomerization with an imaginary frequency of 456i cm^{-1}. Note that there are two TSs on the D_0 surface that are symmetrically located near the LEDP (Figure 4) and have opposite charge-spin separation (i.e., "minus-dot" and "dot-minus"). In the TS geometry shown in Table 2, the half containing the C2 atom carries a negative charge of −0.8035 (state-averaged calculation): in the D_1 state at the same geometry, the negative charge is localized in the other half (−0.9497). Thus, in the section along the DC vector, the minus-dot and dot-minus states cross each other at the LEDP of C_2 symmetry where the two halves have equivalent structures. These TSs are 28.2 kcal mol^{-1} higher for the D_0 stable C_{2v} structure of $MA^{-\bullet}$, but 38.1 kcal mol^{-1} higher for the D_0 stable C_{2h} structure of $FA^{-\bullet}$. This barrier is very low in comparison with the similar perpendicular TSs of PDI, which have been located on the S_0 PES near the S_1/S_0 LEDP [more than 50 kcal mol^{-1} (CASSCF) for both Z- and E-PDI].[27] Then, vibrationally excited $MA^{-\bullet}$ and $FA^{-\bullet}$ on the D_0 PES would be able to reach the transition states. The difference in barrier height of about 10 kcal mol^{-1} between $MA^{-\bullet}$ and $FA^{-\bullet}$ should play an important role after deactivation from the D_1 state. Detailed discussion about this point is in the next section.

From Figure 2, one might expect that $FA^{-\bullet}$ undergoes photoisomerization as well as $MA^{-\bullet}$ does, because the LEDP with a $\theta_1 = 91.2°$ could be equally reached from both the $MA^{-\bullet}$ and $FA^{-\bullet}$ FC regions. However, this is not the case: $DMF^{-\bullet} \rightarrow DMM^{-\bullet}$ photoisomerization has not been observed either in MTHF glass[13] or in aqueous solution.[14] The D_1-state geometry optimization shows that the D_1/D_0 degeneracy begins before approaching $\theta_1 = 91.2°$. When C2−C3 rotation occurs, the θ_2 distortion has to precede the θ_1 distortion because the imaginary frequency of the relaxed structure on the D_1 PES has large components on H1 and H2, as shown in Figure 3.

3.2. Two-Dimensional Analysis of D_1−PES. The results of the two-dimensional PES calculation are shown in Figure 5 along θ_1 and θ_2, which we regard as the cis−trans reaction coordinate and the HOOP motion coordinate, respectively. This relaxed scan was performed in C_2 symmetry using the two-root state-averaged orbital while the two dihedral angles were constrained. The ^2B state was optimized in the area of $0° \le \theta_1 \le 80° \cap 0° \le \theta_2 \le 180°$ (as $MA^{-\bullet}$ side in Figure 5a), and the ^2A state in the area of $100° \le \theta_1 \le 180° \cap 0° \le \theta_2 \le 180°$ (as $FA^{-\bullet}$ side in Figure 5b). The line where the ^2B and ^2A PESs intersect corresponds to the D_1/D_0 hyperline that we have characterized in a previous paper.[10] This intersection lines of Figure 5a,b are sequentially connected through the DP at $\theta_1 = 90°$ and $\theta_2 = 90°$ that has also been already located.[10] This D_1/D_0 hyperline lies well below the Franck−Condon energy.[10] Figure 5 shows that even if θ_1 is not distorted by 91.2°, excited $MA^{-\bullet}$ and $FA^{-\bullet}$ can reach the D_1/D_0 hyperline by θ_2 distortion without barriers. In other words, the deactivation from D_1 to D_0 can be achieved by the θ_2 distortion, i.e., the HOOP motion. This HOOP motion makes it possible for the D_1 excited $MA^{-\bullet}$ and $FA^{-\bullet}$ to transit to D_0 at far points from the LEDP without a large θ_1 distortion. Furthermore, electronic structure becomes its counter isomer upon this deactivation through the HOOP motion though its skeletal structure still remains as the reactant. Besides, the motion along θ_1 and θ_2 does not preserve degeneracy (as shown in Figure 5). This means that the branching plane, which is spanned by GD and DC vectors along the D_1/D_0 hyperline, involves these distortion motions (θ_1 and θ_2). Hence, isomerization is easy via this D_1/D_0 hyperline.

Experimental results[13] show that reactions other than one-way cis → trans photoisomerization were not involved. In contrast, the present PES suggests that mutual cis ↔ trans photoisomerization is possible and that the reverse reaction is not detected experimentally owing to some purely experimental reason(s). The deactivated $MA^{-\bullet}$ and $FA^{-\bullet}$ from the D_1 state via the D_1/D_0 hyperline, however, would have excess energy, i.e., vibrationally hot. According to the present two-dimensional analysis, the D_1 excited $MA^{-\bullet}$ and $FA^{-\bullet}$ can reach the D_1/D_0 hyperline at approximately $\theta_1 = 30°$ and $\theta_1 = 170°$, respectively. This is governed by the topography of CI; i.e., the crossing point where sloped CI becomes intermediate CI or

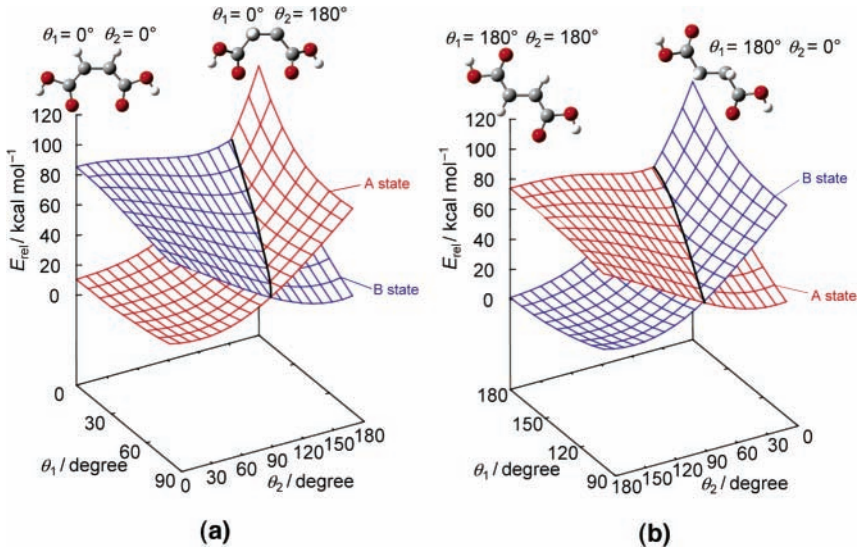

Figure 5. ^{2}A and ^{2}B PES scanned along θ_1 and θ_2 within $0° \le \theta_1 \le 80° \cap 0° \le \theta_2 \le 180°$ (a) (the result of ^{2}B-state optimization) and within $100° \le \theta_1 \le 180° \cap 0° \le \theta_2 \le 180°$ (b) (^{2}A-state optimization). Two PESs cross along the D_1/D_0 hyperline which has been already characterized in ref 10.

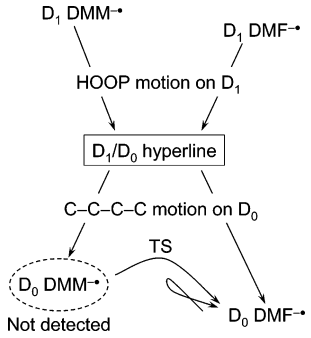

Figure 6. Schematic diagram showing the mechanism of the one-way photoisomerization of $DMM^{-\bullet}/DMF^{-\bullet}$ deduced from the present CASSCF calculation on $MA^{-\bullet}/FA^{-\bullet}$.

peaked CI[28] along the crossing line between ^{2}A and ^{2}B states is regarded as reachable CI. The relative energies of crossing points at $\theta_1 = 30°$ to the D_0 stable $MA^{-\bullet}$ and at $\theta_1 = 170°$ to the D_0 stable $FA^{-\bullet}$ are 47 and 65 kcal mol^{-1}, respectively. Then, at least, these energies can be used in the D_0 state. After the decay from the D_1 to the D_0 state, $FA^{-\bullet}$ can obtain a larger excess energy than $MA^{-\bullet}$ whereas $FA^{-\bullet}$ is forced to travel longer than $MA^{-\bullet}$ on D_0 to their counter isomers because the D_1 excited $FA^{-\bullet}$ can reach the D_1/D_0 hyperline with smaller θ_1 distortion from planar conformation than the D_1 excited $MA^{-\bullet}$. Larger excess energy of $FA^{-\bullet}$ is an offset against the small θ_1 distortion. Similarly, smaller excess energy of $MA^{-\bullet}$ is an offset against the large θ_1 distortion. This situation implies that the difference in available excess energy in the D_0 state would not be a determining factor of one-way reaction. Available excess energy, however, should be an important factor.

To isomerize using the excess energy, it is necessary to overcome the energy barrier at the TS (see Figures 2 and 4) that is the barrier in cis ↔ trans isomerization in the D_0 state. From the present CASCF result, this barrier, which marks the boundary between cis and trans forms, is significantly low in comparison with that between *Z* and *E* forms of PDI.[27] Then, the following scenario can be suggested for the one-way photoisomerization: The hot $MA^{-\bullet}$ can overcome the barrier, which is 28 kcal mol^{-1} with respect to the D_0 minimum $MA^{-\bullet}$, whereas the hot $FA^{-\bullet}$ cannot because the barrier height is 37 kcal mol^{-1} with respect to the D_0 minimum $FA^{-\bullet}$. The difference of barrier height stems from the steric repulsion that we have already mentioned. That is to say, in $MA^{-\bullet}$, there is a strong repulsive interaction between the two carbonyl oxygens, as is reflected in the large C1−C2−C3 and C2−C3−C4 bond angles. In contrast, there is no steric repulsion in $FA^{-\bullet}$. Consequently, this steric repulsion makes $MA^{-\bullet}$ more unstable than $FA^{-\bullet}$ on the D_0 PES, resulting in the energetic difference in the activation energy seen by cis and trans forms. Indeed, that difference has been experimentally detected that a rapid electrochemically induced $DMM^{-\bullet}$ (cis form) → $DMF^{-\bullet}$ (trans from) one-way isomerization process takes place at room temperature.[16,17] Namely, this system of $MA^{-\bullet}/FA^{-\bullet}$ undergoes the one-way isomerization without UV illumination. If D_1 excited molecules can reach the D_1 minimum corresponding to the D_1/D_0 LEDP, mutual cis ↔ trans photoisomerization should be detected. However, D_1 excited molecules can transit to D_0 at the far points from the LEDP by the HOOP motion. Hence, the $MA^{-\bullet}/FA^{-\bullet}$ deactivated by HOOP motion is forced to travel up to its isomer in the D_0 state. UV light illumination produces vibrationaly hot $MA^{-\bullet}/FA^{-\bullet}$ by the transition via the D_1/D_0 hyperline.

In most photoreaction systems, available products usually depend on the initial conditions and excited-state PES topography.[29] In contrast, in the present system, the initial conditions on the excited state are blurred out and the final product only depends on the ground-state PES topography because the photoenergy is once transferred to vibrational energy.

4. Conclusion

We have found that, even if the molecular skeleton that decides the cis or trans form, i.e., the C1−C2−C3−C4 dihedral angle in this paper, does not largely distort, the photoisomerization occurs by the distortion of the H1−C2−C3−H2 dihedral angle (corresponding to the HOOP motion). Moreover, we suggested the following two-step isomerization mechanism. First, H1−C2−C3−H2 dihedral angle distortion occurs on the D_1 PES. Second, C1−C2−C3−C4 dihedral angle distortion occurs on the D_0 PES. Therefore, D_0, not D_1, is responsible for the one-way photoisomerization. This result well corresponds to the recent experiment about the photoisomerization of 11-cis to all-trans RPSB where HOOP is detected at an early stage after light illumination.[20]

Recent theoretical calculation about the model molecule of RPSB have shown the large possibility that a perpendicular S_1/S_0 DP is involved in the photoisomerization.[25] Considering that both olefin ion radicals such as $MA^{-\bullet}/FA^{-\bullet}$ in this paper and highly polar double-bond systems such as RPSB have the analogous perpendicular DP corresponding to the minimum of the first excited state, the PES of $MA^{-\bullet}/FA^{-\bullet}$ is expected to be similar to that of RPSB. Therefore, in these systems, the two-step isomerization suggested in this paper would be general: first HOOP (H−C−C−H dihedral angle distortion) on excited-state surface occurs, and then the large fraction of the net motion along the isomerization coordinate on the ground-state surface.

The C1−C2−C3−C4 dihedral angle usually decides the cis or tans form. The distortion of this dihedral angle occurs on the D_0 PES. We predicted that the D_0 state is responsible for the one-way isomerization. The experimental results can be interpreted by assuming there is the TS on the D_0 state that the cis form can overcome whereas the trans form cannot.[16,17] The suggested mechanism for the one-way photoisomerization of $DMM^{-\bullet}/DMF^{-\bullet}$ is summarized in Figure 6.

Acknowledgment. We are grateful to Dr. Ohgi Takahashi for a stimulating discussion.

Supporting Information Available: The most stable structure of $DMM^{-\bullet}$ and $DMF^{-\bullet}$ in the D_0 state is discussed, including a figure of considered conformations, tables of energies, S^2 values, and Cartesian coordinates. This material is available free of charge via the Internet at http://pubs.acs.org.

References and Notes

(1) Migani, A.; Olivucci, M. Conical Intersection and Organic Reaction mechanisms. In *Conical Intersections: Electronic Structure, Dynamics & Spectroscopy*; Advance Series in Physical Chemistry Vol. 15; Domcke, W., Yarkony, D. R., Koppel, H., Eds.; World Scientific: Singapore, 2004; p 271.

(2) Blancafort, L.; González, D.; Olivucci, M.; Robb, M. A. *J. Am. Chem. Soc*. **2002**, *124*, 6398.

(3) Yarkony, D. R. Conical Intersection: Their Description and Consequences. In *Conical Intersections: Electronic Structure, Dynamics & Spectroscopy*; Advance Series in Physical Chemistry Vol. 15; Domcke, W., Yarkony, D. R., Koppel, H., Eds.; World Scientific: Singapore, 2004; p 41.

(4) Bernardi, F.; Olivucci, M.; Robb, M. A. *Chem. Soc. Rev*. **1996**, *25*, 321.

(5) Ragazos, I. N.; Robb, M. A.; Bernardi, F.; Olivucci, M. *Chem. Phys. Lett.* **1992**, *197*, 217.

(6) Bearpark, M. J.; Robb, M. A.; Schlegel, H. B. *Chem. Phys. Lett.* **1994**, *223*, 269.

(7) Dallos, M.; Lischka, H.; Shepard, R.; Yarkony, D. R.; Szalay, P. G. *J. Chem. Phys*. **2004**, *120*, 7330.

(8) Migani, A.; Robb, M. A.; Olivucci, M. *J. Am. Chem. Soc*. **2003**, *125*, 2804.

(9) Venturini, A.; Vreven, T.; Bernardi, F.; Olivucci, M.; Robb, M. A. *Organometallics* **1995**, *14*, 4953.

(10) Takahashi, O.; Sumita, M. *J. Chem. Phys*. **2004**, *121*, 7030.

(11) Takahashi, O.; Sumita, M. *J. Mol. Struct.*: *THEOCHEM* **2005**, *731*, 173.

(12) (a) Ben-Nun, M.; Martinez, T. *J. Chem. Phys*. **2000**, *259*, 237 (b) Ruiz, D. S.; Cenbran, A.; Garavelli, M.; Olivucci, M.; Fuss W. *Photochem. Photobiol*. **2002**, *76*, 622. Hunt, P. A.; Robb, M. A. *J. Am. Chem. Soc*. **2005**, *127*, 5720.

(13) Torikai, A.; Suzuki, T.; Miyazaki, T.; Fueki, K.; Kuri, Z. *J. Phys. Chem*. **1971**, *75*, 482. Torikai, A.; Nakano, F.; Fueki, K.; Kuri, Z. *Bull. Chem. Soc. Jpn*. **1975**, *48* 339.

(14) Hayon, E.; Simic, M. *J. Am. Chem. Soc.* **1973**, *95*, 2433.

(15) Shida, T.; Hamill, W. H. *J. Chem. Phys*. **1966**, *44*, 4372.

(16) Nelsen, S. F. *Tetrahedron Lett*. **1967**, *39*, 3795.

(17) Doherty, A. P.; Scott, K. J. *Electoanal. Chem*. **1998**, *442*, 35.

(18) Takahashi, O.; Kikuchi, O. *J. Chem. Phys*. **1994**, *100*, 1350.

(19) Yarkony, D. R. *Acc. Chem. Res.* **1998**, *31*, 511.

(20) Kukura, P.; McCamant, D. W.; Yoon, S.; Wandschneider, D. B.; Mathies, R. A. *Science* **2005**, *310*, 1006.

(21) Matos, M. A. R.; Miranda, M. S.; Morais, V. M. F.; Liebman, J. *F. Org. Biomol. Chem*. **2003**, *1*, 2930. Maçôas, E. M. S.; Fausto, R.; Lundell, J.; Pettersson, M.; Khriachtchev, L.; Räsänen, M. *J. Phys. Chem*. A **2001**, *105*, 3922. George, W. O.; Porter, A. J. *J. Chem. Soc., Perkin II* **1973**, 954. Compton, D. A. C.; George, W. O.; Porter, A. J. *J. Chem. Soc., Perkin II* **1975**, 400. Buge, H. G.; Peich, P.; Steger, E. *J. Mol. Struct*. **1976**, *35*, 175.

(22) I. Elson, H.; Kemp, T. J.; Greatorex, D.; Jenkins, H. D. B. *J. Chem. Soc., Faraday Trans*. **1973**, *69*, 1402. Nelsen, S. F.; Gillespie, J. P. *J. Org. Chem*. **1975**, *40*, 2391.

(23) Frisch, M. J.; Trucks, G. W.; Schlegel, H. B.; Scuseria, G. E.; Robb, M. A.; Cheeseman, J. R.; Zakrzewski, V. G.; Montgomery, J. A., Jr.; Stratmann, R. E.; Burant, J. C.; Dapprich, S.; Millam, J. M.; Daniels, A. D.; Kudin, K. N.; Strain, M. C.; Farkas, O.; Tomasi, J.; Barone, V.; Cossi, M.; Cammi, R.; Mennucci, B.; Pomelli, C.; Adamo, C.; Clifford, S.; Ochterski, J.; Petersson, G. A.; Ayala, P. Y.; Cui, Q.; Morokuma, K.; Malick, D. K.; Rabuck, A. D.; Raghavachari, K.; Foresman, J. B.; Cioslowski, J.; Ortiz, J. V.; Stefanov, B. B.; Liu, G.; Liashenko, A.; Piskorz, P.; Komaromi, I.; Gomperts, R.; Martin, R. L.; Fox, D. J.; Keith, T.; Al-Laham, M. A.; Peng, C. Y.; Nanayakkara, A.; Gonzalez, C.; Challacombe, M.; Gill, P. M. W.; Johnson, B. G.; Chen, W.; Wong, M. W.; Andres, J. L. M.; Head-Gordon, M.; Replogle, E. S.; Pople, J. A. *Gaussian 98*, revision A.11.3; Gaussian, Inc.: Pittsburgh, PA, 1998.

(24) Andresson, K.; Roos, B. O. Multiconfigurational second-order perturbation theory. In *Modern Electronicl Structure Theory Part I*; Advance Series in Physical Chemistry Vol. 2; Yarkony, D. R., Ed.; World Scientific: Singapore, 1995; p 55.

(25) Garavelli, M.; Celani, P.; Bernardi, F.; Robb, M. A.; Olivucci, M. *J. Am. Chem. Soc.* **1997**, *119*, 6891. Garavelli, M.; Vreven, T.; Celani, P.; Bernardi, F.; Robb, M. A. *J. Am. Chem. Soc.* **1998**, *120*, 1285.

(26) Takahashi, O.; Kikuchi, O. *J. Mol. Struct.*: *THEOCHEM* **1994**, *313*, 207. Oshiyama, T.; Takahashi, O.; Morihashi, K.; Kikuchi, O.; Tokumaru, K. *Bull. Chem. Soc. Jpn.* **1993**, *66*, 1622. Kikuchi, O.; Oshiyama, T.; Takahashi, O.; Tokumaru, K. *Bull. Chem. Soc. Jpn.* **1992**, *65*, 2267.

(27) Sumita, M.; Saito, K. Manuscript in preparation.

(28) Bischof, G. J.; Xantheas, S. S.; Ruedenberg, K. *J. Chem. Phys*. **1991**, *95*, 1862.

(29) Hettema, H.; Yarkony, D. R. *J. Chem. Phys*. **1995**, *102*, 8431.